Turbulent flow field comparison and related suitability for fish passage of a standard and a simplified low-gradient vertical slot fishway

# Turbulent flow field comparison and related suitability for fish passage of a standard and a simplified low-gradient vertical slot fishway

Numerical simulations of vertical slot fishways

Quaranta E.[1], Katopodis C[2]., Revelli R[3]., Comoglio C.[4]

[1 4], *Politecnico di Torino, DIATI (Department of Environment, Land and Infrastructure Engineering).*
*Corso Duca degli Abruzzi 24, 10129, Torino, Italia*

[3], *Politecnico di Torino, DIATI and Duke University (USA).*

[2] *Katopodis Ecohydraulics Ltd., Winnipeg, Canada*

**Abstract**

Fishways are hydraulic structures that allow passage of fish across obstructions in rivers. Vertical slot fishways -VSF- are considered the most efficient and least selective type of technical fishway solutions, especially due to their ability to remain effective even when significant upstream and/or downstream water level fluctuations occur. The scope of the present study is to perform numerical simulations in order to investigate and compare the hydraulic turbulent flow field in a standard and a simplified version of the most common VSF design. Implications in relation to fish swimming behavior and fish passage performance are discussed.

*[1](corresponding author). emanuele.quaranta@polito.it, Tel: 0039 0110905682
**[2]KatopodisEcohydraulics@live.ca
[3]roberto.revelli@polito.it
[4] claudio.comoglio@polito.it

Different water depths (as well as discharges) were investigated, using a bed slope of 5%, as a reference for low-gradient VSFs with a very limited selectivity that can be used in multispecies rivers in grayling-barbel regions. Results show that maximum values of velocity, turbulent kinetic energy and Reynolds stresses are higher in the standard design. However, corresponding to slot geometry and orientation, the direction of the main jet in the simplified design is more inclined towards the left side of the pool. This causes the eddy to split into two smaller ones; the minimum eddy dimension is reduced from 0.4-0.5 m to 0.2-0.3 m. These dimensions are detrimental for fish passage efficiency, being more comparable with fish length (0.15-0.40 m), thus affecting migrating fish stability and orientation. Furthermore, the standard design provides a more straightforward upstream path and wider areas of low flow velocities and turbulence, useful for fish resting. Therefore, it is recommended that the standard design should be preferred over its simplified version, even if its construction costs are around 10-15% higher than the simplified one.

*Keywords:* CFD, ecohydraulics, fish passage, fishway, vertical slot fishway

## 1. Introduction

Throughout the world, anthropogenic obstructions in rivers have generated relevant adverse effects on fish migratory routes. The interruption of longitudinal connectivity of a natural river is perceived as one of the main causes in the decline of freshwater ichthyofauna (Calles and Greenberg, 2009).

In order to restore to an acceptable level the longitudinal connectivity

of a river fragmented by man-made obstacles, the construction of effective fishways represents the best practice where obstacle removal is not feasible. Fishways are hydraulic structures designed to allow passage of upstream migrating fish through river obstructions, such as weirs or dams. Pool-type are the most common fishway used worldwide (Bunt et al., 2012; Hatry et al., 2013; Santos et al., 2012). Pool-type fishways consist of a channel with a sloping bed that is divided into a series of pools by cross-walls at regular intervals.

Different fishway geometries lead to different hydraulic flow fields, and, as a consequence, a certain typology will likely be more suitable for some species and fish lengths, and less for others. Hence the design of a fishway has to take into account the swimming capability, size and behavior of the species of concern (Clay, 1995; Katopodis and Williams, 2012; Katopodis and Gervais, 2016).

### *1.1. Fish and flow field interaction*

The flow field in a fishway affects species behavior, and the capability of fish to successfully migrate through it. Indeed, the flow field generates shear stresses and hydrodynamic resistance on fish, making migration an energetically demanding process. Hence fishway design needs to be based on biological characteristics of the fish species that are expected to migrate upstream of the considered obstacle, with particular regard to their morphology, behavior and swimming ability. Maximum allowed flow velocity value (occurring in the slot) is defined based on the burst speed of the weakest fish species expected to migrate. Together with body size of the largest migrants, it constitutes a significant parameter affecting fishway di-

mensions and related construction costs (mainly related to bottom slope and pool dimensions).

When passing from one pool to the upstream one, fish can reach burst speed; this is the top speed, which lasts for a few seconds, by the exclusive utilization of white muscles (Plaut, 2001). Flow velocity creates hydrodynamic resistance to fish, and when it exceeds burst speed, migration can be seriously compromised. Therefore, the maximum upstream migration distance diminishes as flow velocity increases (Katopodis and Gervais, 2016). For example, it is estimated that distance traveled by cyprinids and salmonids decreases for flow velocities higher than 1.5 m/s, that are typical velocities encountered by fish when passing from one pool to the next one (Puertas et al., 2012). Hence fish need resting areas, characterized by lower flow velocities (e.g. velocities of 0.2-0.4 m/s are recommended values for cyprinids-Iberian barbel), for a short resting before a subsequent upstream movement through higher velocity areas (Silva et al., 2011).

Also turbulence affects fish behavior. The most relevant turbulent variables are turbulent kinetic energy ($TKE$), eddies diameter and Reynolds stresses ($RS$) (Silva et al. 2012; Silva et al., 2015).

$TKE$ (kinetic energy associated with fluctuating components of the velocity) affects fish swimming performance by increasing swimming costs. High $TKE$ can confuse fish in their efforts to move though the fishway along energy efficient paths, increasing fish fatigue. Silva et al. (2011) have noticed that Iberian barbel used low $TKE$ locations (TKE$\leq$0.05 m$^2$/s$^2$) as resting areas before subsequent efforts to traverse areas of higher velocity and turbulence (i.e. along the main jet). Therefore, a large portion of the

pool should stay below $TKE \leq 0.05$ m$^2$/s$^2$. This means that in low velocity areas also low $TKE$ values should be provided.

Shear stresses and Reynolds stresses $RS$ ($RS$ are shear stresses generated by fluctuations in velocity over time due to turbulence, while shear stresses are generated by fluid viscosity) affect fish swimming performance and stability, and can even cause injury or mortality (Silva et al., 2011; Silva et al., 2012; Silva et al., 2015). In Silva et al. (2011), it has been observed that on the horizontal plane barbel occupied positions with absolute $RS \leq 60$ N/m$^2$. Thus $RS \leq 60$ N/m$^2$ can be considered a reference threshold.

Furthermore, the diameter of eddies forming in the fishway flow plays an important role. The interaction with eddies is a complex phenomenon that results from the capacity of fish to integrate biomechanics, physiological and sensory processes (Marriner at al., 2016). If eddies are significantly smaller than fish size, fish may swim steadily through them. Eddy diameters close to the length of migrating fish, particularly in combination with high eddy vorticity, can affect fish stability and result in reduced fishway performance. When eddy size is larger than fish total length, fish orientation disturbance is minimal (Silva et al., 2012; Tritico and Cotel, 2010).

Therefore, based on the aforementioned scientific literature, it is recommended that resting zones with $TKE \leq 0.05$ m$^2$/s$^2$ and $RS \leq 60$ N/m$^2$ be provided in 30% to 50% of the pool, with velocities kept under 0.30 m/s, keeping eddies dimensions to adequate values compared to upstream migrants body lengths.

### *1.2. Vertical slot fishways*

Vertical slot fishways -VSF- are considered the most efficient and least selective type of technical fish pass solutions, especially due to their ability to remain effective even when significant upstream and/or downstream water level fluctuations occur. The velocity field in the pools is relatively insensitive to flow rate variations (Katopodis, 1992). VSF are recommended especially in rivers where several fish species with different swimming capabilities are present (FAO and DVWK, 2002). VSFs basically consist of a sloping rectangular channel divided into a number of pools by vertical baffles. Water flows through the vertical slot between the baffles, from one pool to the downstream one. The water level difference between two adjacent pools depends on the slope of the fishway and on the length of the pool.

Rajaratnam et al. (1992) evaluated eighteen different designs of VSF using physical models. In particular, Design 1 is the most common design (a standard reference commonly used in real applications), while Design 16 is its simplified version, and it represents a low cost option for the construction of a VSF (see Fig.1). The slot orientation, i.e. the angle between the width of the slot and the longitudinal direction, is $\alpha = 45°$ for Design 1 and $\alpha = 34°$ for Design 16. The two designs differ also on the shape of the baffles, as it can be seen in Fig.1. The baffle shape of Design 1 is more complex, leading to higher construction costs.

Conventionally, analysis of VSFs hydrodynamics and their design have been performed using physical models (Rajaratnam et al., 1992; Wu et al., 1999; Puertas et al., 2004), whereas field experiments have been con-

ducted for evaluating fish passage efficiencies (Laine et al., 1998; Stuart and Berghuis, 2002). In recent decades, improvements in computer technology and numerical algorithms, have allowed computational fluid dynamics (CFD) to be increasingly used for hydraulic problems, including fishways. For example, in Khan (2006) and Marriner et al. (2014), 3D CFD simulations of VSF have been performed, solving the 3D RANS (Reynolds Average Navier Stokes) equations.

The scope of the present work is to show a detailed comparison and flow field description of the two vertical slot fishway designs. The main objective is to understand through the use CFD tools, if the simplified design, whose construction costs are generally 10-15% lower (based on personal communications about cost estimates collected from four construction firms), can have the same effectiveness as the standard one.

Model results for the two designs were compared with reference to representative turbulent flow field parameters (e.g. $TKE$, $RS$, see section 1.1) identified as the most influential on fish passage by the latest experimental studies. Furthermore, the 3D modeling was carried out with the aim of analyzing possible changes in the turbulent flow field generated at varying depths along the two typologies of VSF.

## 2. Method

### *2.1. Geometry*

The geometric design of the two typologies of VSF is depicted in Fig.1, using a slot width $b_0 = 0.30$ m. The length and width of the pool are $L = 10b_0$ and $b = 8b_0$, respectively; these are established across North

America and Europe as the recommended design dimensions for regular pools (Marriner et al., 2016). These correspond to a pool length of 3 m and a pool width of 2.4 m.

In order to find an optimal compromise between accuracy and computational cost, five pools were simulated (pools were named pool 2-3-4-5-6 from upstream to downstream), with a 6 m long headrace (pool 1) and a 6 m long tailrace (pool 7), where inlet/outlet boundary conditions were imposed, respectively. Results are discussed in relation to pool 4 which is used as a reference for a typical pool. In pool 4 the flow field can be considered the representative one, also for a VSF with a bigger number of pools (as confirmed in Khan, 2006; Heimerl et al., 2008).

The adopted bed slope is 5%, which is considered an appropriate value for multispecies rivers to limit species selectivity (Katopodis and Williams, 2012; Schmutz and Mielach, 2013). Therefore, the analyzed VSF is considered as a low-gradient fishway by international standards (White et al., 2011). Considering a pool length of 3 m, the head drop between two pools is 0.15 m, which is a suitable value for a wide variety of fish species in barbel-grayling regions, including large migrants such as Danube salmon and Northern pike (Schmutz and Mielach, 2013).

### *2.2. Hydraulic conditions*

Considering the relationship linking the water depth at the center of the pool $y_0$ with the flow rate (Rajaratnam et al., 1992), flow rates corresponding to values $y_0 = 1$ m, $y_0 = 1.5$ m and $y_0 = 2$ m were used to investigate possible changes of the turbulent flow field at varying water depths (as well as flow rates). Using three different values of $y_0$ means that, for each design,

three different flow rate conditions were simulated. Using the bed slope of 5%, and the equations reported in Rajaratnam et al. (1992), flow rates were $Q = 0.395$ m$^3$/s, $Q = 0.612$ m$^3$/s and $Q = 0.829$ m$^3$/s for Design 1, and $Q = 0.413$ m$^3$/s, $Q = 0.619$ m$^3$/s and $Q = 0.826$ m$^3$/s for Design 16. The generated flow rates are similar for the two designs, with slight differences due to the dissimilar flow field generated by the altered geometry.

Following the approach reported in Khan (2006), planes parallel to the bed were used for the description of the flow field. In Khan (2006), the following planes were used: the deepest ones were $H_1$ at $y/y_0 = 0.05$ and $H_2$ at $y/y_0 = 0.33$ (these represent the flow field for bottom oriented fish species). In contrast, planes $H_4$ at $y/y_0 = 0.67$ and $H_5$ at $y/y_0 = 0.95$ represent the flow field faced by fish swimming in the upper portion of the water column. The last plane is $H_3$ at $y/y_0 = 0.5$. The components of velocity normal to these planes were negligible, as shown in Wu et al. (1999): this is an expected result for bed slopes lower than 10%.

### *2.3. Mesh*

A tetrahedral computational mesh was generated, which becomes hexahedral when approaching the bed. The mesh cell dimensions ranged from 0.025 m at the walls to 0.05 m in the pools. These values are comparable and finer with respect to those adopted in Khan (2006) -0.025 to 0.100 m-, and in Marriner et al. (2014) -0.11 m-. Considering the dimensions of the hydraulic flow field structure typical of such fishways (e.g. eddies), these cell dimensions can be considered adequate for simulating the flow field affecting fish behavior.

### *2.4. CFD model: setup*

Reynolds Averaged Navier–Stokes (RANS) equations were solved by the software FLUENT to simulate the average flow field. Three momentum equations (one equation for each cartesian coordinate) and the continuity equation were solved. The VOF (Volume of Fluid) method was used to determine the free surface position (Olsson et al. 2007).

For an incompressible fluid the continuity equation is:

$$\frac{\partial U_i}{\partial x_i} + \frac{\partial U_j}{\partial x_j} + \frac{\partial U_w}{\partial x_w} = 0 \tag{1}$$

where $x_i$, $x_j$ and $x_w$ are the directions of the cartesian reference coordinate system. The generic $U_y = \frac{1}{T}\int_t^{t+T} u_y dt$ is the time averaged velocity (see eq. 2) in $x_y$ direction, where $u_y$ is the instantaneous flow velocity, $t$ is the time and $T$ is the integration time interval ($y$ can be $i$, $j$ or $w$). In an analogous way, $P = \frac{1}{T}\int_t^{t+T} p dt$, with $p$ the instantaneous pressure.

The momentum equation in direction $x_i$, is:

$$\rho\left(\frac{\partial U_i}{\partial t} + U_i\frac{\partial U_i}{\partial x_i} + U_j\frac{\partial U_i}{\partial x_j} + U_w\frac{\partial rU_i}{\partial x_w}\right) = \rho g_i - \frac{\partial P}{\partial x_i} + \mu\nabla^2 U_i + \frac{\partial \tau_{i,i}}{\partial x_i} + \frac{\partial \tau_{i,j}}{\partial x_j} + \frac{\partial \tau_{i,w}}{\partial x_w} \tag{2}$$

where $\rho$ and $\mu$ are density and dynamic viscosity of the fluid, $g$ is the gravitational acceleration, $P$ is the time averaged pressure and $U_i$ is the time averaged velocity of the mixture along direction $x_i$. Analogous momentum equations are solved along directions $x_j$ and $x_w$. The absolute flow velocity

is $U = \sqrt{{U_i}^2 + {U_j}^2 + {U_w}^2}$.

The terms $\tau_{i,j}$ are the Reynolds turbulent stresses ($RS$), and they can be expressed as:

$$\tau_{i,j} = -\rho\overline{u_i' u_j'} = \mu_t \left( \frac{\partial U_i}{\partial x_j} + \frac{\partial U_j}{\partial x_i} \right) - \frac{2}{3}\rho k \delta_{ij} \tag{3}$$

where $\mu_t$ is the turbulent dynamic viscosity, $k$ is the turbulent kinetic energy and $\delta_{ij}$ is the Kronecker delta. The fluctuating component $u_i'$ of velocity in direction $i$ is the difference between the instantaneous value of velocity and the average velocity $U_i$.

The turbulent dynamic viscosity is calculated using the $k - \epsilon$ model, where the turbulent viscosity is expressed as a function of turbulent kinetic energy $k$ and turbulent dissipation $\epsilon$.

$$\mu_t = \rho C_\mu \frac{k^2}{\epsilon} \tag{4}$$

where $C_\mu = 0.09$.

Turbulent kinetic energy is defined as $TKE = 1/2[{u_i'}^2 + {u_j'}^2 + {u_w'}^2]$.

The pressure-velocity coupling was solved by PISO (Pressure Implicit with Splitting of Operator) scheme. Spatial discretizations were realized by the following schemes: PRESTO for pressure and QUICK for momentum and turbulent kinetic energy, in alignment with Barton et al. (2008). The Curvature correction was added to sensitize the model to streamline curvatures. The numerical simulations were run in stationary conditions. This numerical model has been successfully used in Quaranta et al. (2016), using a bed slope of 10% and flow rate of 1.20 $m^3/s$.

When analyzing the results (section 3), average values of flow velocity, $TKE$ and $RS$ in the jet and in resting areas were evaluated. Considering flow velocity, the average values were calculated as $\overline{U_s} = \frac{1}{S_{sides}} \sum^{S_{side}} UdS$ and $\overline{U_{jet}} = \frac{1}{S_{jet}} \sum^{S_{jet}} UdS$, where $U$ is the time average flow velocity, $dS$ is the infinitesimal area (in this case it is the area of each cell of the mesh) $S_{side}$ is the area of the pool side and $S_{jet}$ is the area of the jet. In an analogous way, this process was applied to $TKE$ and $RS$ in addition to $U$.

*2.4.1. Boundary conditions*

At the water inlet, a fixed value of turbulence intensity $I = \frac{\sqrt{{u'_i}^2+{u'_j}^2+{u'_w}^2}}{U} = 0.05$, with $U$ the average flow velocity, and a fixed value of turbulent viscosity ratio $\mu_t/\mu = 10$ were specified, where $\mu_t$ is the turbulent dynamic viscosity and $\mu$ is the water dynamic viscosity. This intensity is considered a common value used in such type of simulations (Quaranta and Revelli, 2016), and higher values do not affect the flow field (Marriner et al., 2014). The flow rate was imposed at the inlet, as previously described. At the water outlet a fixed water depth was provided in order to ensure the required $y_0$ ($y_0 = 1.0$ m, $y_0 = 1.5$ m, $y_0 = 2.0$ m).

## 3. Results

Planes parallel to the bed were used for the description of the flow field. In the following sections, reference will be made predominantly to planes $H_2$ and $H_4$, since these planes can be considered the most representative locations for analyzing the flow field.

### *3.1. Topology of the flow field*

The results obtained in this study for a bed slope of 5% showed that the flow field was characterized by a main water jet between the slots, with the generation of one eddy on the right and one eddy on the left side of the pool. Due to the orientation of the slot ($\alpha$ in Fig.1), the jet was not straight, but curved toward the left side of the pool. Furthermore, in Design 16 a small eddy was generated on the right side of the upstream pointed baffle (see Figs. 2, 3, 4). The capability of the model to capture this small eddy confirmed its good performance. Figures 2, 3, 4 show the velocity flow field of Design 1 and Design 16 for the three water depth values, and along the investigated planes.

In Design 1 the jet exited from the slot at an angle of 45°. Its orientation with respect to the longitudinal direction after the slots became 29°, due to its curved shape, and then it was quite straight toward the downstream slot. This shape was practically constant along the vertical direction. The most appreciable 3D characteristic was that maximum jet velocity decreased as it approached the free surface, and jet width became slightly larger.

Considering Design 16, the hydraulics were similar to Design 1. However, in this case the jet between the slots was more curved, 36° vs 29°, just downstream of the slot, due to the different slot orientation, and this characteristic generated significant differences between the two designs.

The first effect (a) is that the length of the water jet was longer in Design 16 ($l \simeq 1.2L$) than the length of the jet in Design 1 ($l \simeq 1.1L$). Furthermore, (b) in Design 1 the right eddy was more elongated in the longitudinal direction, while in Design 16 the shape of the eddy on the right

approached a more circular shape. The most important consequence (c) attributed to the larger jet orientation angle in Design 16 was the splitting of the eddy on the left of the pool into two smaller ones, for all the investigated flow rates. The last effect (d) is that the jet in Design 16 affected the left side of the pool (the left side was larger than the right side) more than in Design 1, reducing the width of resting zones.

### *3.2. Flow velocity of jet and resting areas*

Table 1 reports for each design and flow rate (as well as $y_0$), the maximum flow velocity $U_{max}$ (that occurred in the jet just downstream of the slot), the average velocity at pool sides ($\overline{U_s}$, i.e. the average flow velocity of areas located outside the main jet) and along the jet ($\overline{U_{jet}}$). The percentage of pool area $A$ where the flow velocity in the cell of the mesh was lower than 0.3 m/s, was quantified.

With regards to the jet, maximum velocity ($U_{max}$) and average jet velocity ($\overline{U_{jet}}$) decreased as flow rate increased (hence with $y_0$ increase).

In both designs, maximum flow velocity $U_{max}$ decreased approaching the free surface; maximum flow velocity on $H_4$ was about 5.7% (Design 1) and 6.5% (Design 16) lower than maximum flow velocity on $H_2$ (the width of the jet spread approaching the free surface). This was valid when $y_0 = 1$ m and $y_0 = 1.5$ m, while when $y_0 = 2$ m maximum flow velocity decrease was only about 1%. In both designs, $U_{max}$ decreased of 7-13% (Design 1) and 2-3% (Design 16) passing from $y_0 = 1$ m to $y_0 = 1.5 - 2$ m (hence by increasing flow rate), on both planes.

In Design 1, the decrease of $u_{jet}$ was 4-10% passing from $y_0 = 1$ m to $y_0 = 1.5 - 2$ m on $H_2$, but 3-6% when considering the decrease of $u_{jet}$ with

$y_0$ on $H_4$. When considering Design 16, the decrease of $u_{jet}$ was 4-13% passing from $y_0 = 1$ m to $y_0 = 1.5 - 2$ m on $H_2$, and it was negligible on $H_4$.

Average flow velocity in the resting areas ($\overline{U_s}$) reduced when the free surface was approached; $\overline{U_s}$ on $H_4$ was lower than on $H_2$ of 9-15%. On $H_2$, $\overline{U_s}$ increased with flow rate (as well as $y_0$); the increase was 10% for Design 1, but for Design 16 no specific trend was identified.

Comparing the two designs, maximum velocity magnitude was lower in Design 16 with respect to Design 1. The difference was about 12% for $y_0 = 1$ m and about 3% for $y_0 = 2$ m. Average jet velocity was lower in Design 16 of about 1-5% on $H_2$, and 8-11% on $H_4$. Instead, $\overline{U_s}$ was appreciably higher in Design 16 of more than 16% with respect to Design 1, except for $y_0 = 2$ m, whose differences were negligible.

The area percentage $A$ remained substantially constant in Design 1 (at different $y_0$ and depths), while it was more variable in Design 16, due to the more variable flow field (vortex splitting). The area $A$ was generally wider in Design 1, as it can be observed from Table 1. On the other hand, on the plane $H_4$ for $y_0 > 1$ m, $A$ was wider in Design 16, and in this case the differences were more appreciable (11%, which corresponded to 0.7 m$^2$, Table 1). Under these conditions, the vortex splitting almost disappeared, while a larger vortex appeared instead of two smaller and faster eddies, contributing to a global decrease of velocity. The resting areas $A$ were restricted to between 30% and 50% of the pool.

### *3.3. Eddy shape and dimensions*

With regards to eddy shape and dimensions, the two designs exhibited different behavior. The jet angle $\alpha$ (Fig.1) was7° smaller in Design 16, leading to a jet more inclined toward the left side of the pool (Fig.1). The eddy on the left was more elliptical, while the eddy on the right tended to approach a circular shape. This can be observed in Figs. 2, 3, 4. As previously described, this eddy on the left under some conditions split into two smaller ones.

Since jet orientation increased slightly with the vertical coordinate, the vortex splitting occurred in the uppermost part of the pool, and therefore the flow behavior moved from 2D to 3D in Design 16 (Fig.5). This again shifts the design choice to Design 1. The jet orientation reduced slightly with increasing flow rate (i.e. $y_0$); therefore, the higher the flow rate, the less developed was the vortex splitting. This can be observed looking at Figs. 2, 3, 4; in Fig. 2, the vortex splitting was well developed, while it was not in Fig.4, where the flow rate is higher. As a consequence, the minimum relative depth $y/y_0$ from which the vortex splitting began, increased with the increase in flow rate. When $y_0 = 1.0$ m two eddies were already generated at $y/y_0 = 0.33$; when $y_0 = 1.5$ m the presence of two eddies started at $y/y_0 = 0.5$, and the vortex splitting occurred only near the free surface when $y_0 = 2.0$ m. A representative case of eddy splitting can be seen in Fig.5, where the flow field is reported at different planes.

All the eddies presented a core zone, with very low velocity (lower than 0.1 m/s), and a swirling flow around the rotating core. Table 2 shows the maximum and minimum dimensions of each eddy core. Where the eddy

splitting occurred, the smallest eddy is considered.

For Design 1, the maximum eddy dimension, generally along the longitudinal direction, was usually more than twice the smaller one. On the left side of the pool, the longitudinal eddy dimension was 0.75-1.05 m, while the transversal one was 0.27-0.54 m. On the right side, dimensions were 0.42-0.71 m in the longitudinal direction and 0.16-0.21 m in the transversal one.

Eddy dimensions slightly reduced as the free surface was approached. This can be seen in Table 2, comparing for each $y_0$ longitudinal and transversal eddy dimensions on plane $H_2$ and $H_4$. The difference was generally less than 10% with respect to the average dimension (the average dimension was the average between the dimension measured on plane $H_2$ and $H_4$).

Considering Design 16, due to the eddy splitting, the core of eddies was smaller. On the left side of the pool, the longitudinal eddy dimension was 0.52-0.90 m, while the transversal one was 0.22-0.42 m. On the right side, dimensions were 0.33-0.69 m in the longitudinal direction and 0.22-0.38 m in the transversal one. Furthermore, left eddy maximum dimension enlarged with increasing $y_0$, since the eddy splitting started at a relative depth $y/y_0$ closer to the free surface as $y_0$ increased. This means that the two smaller eddies progressively disappeared merging into one bigger vortex.

### *3.4. Turbulent kinetic energy in the pools*

Figure 6 depicts an overview of $TKE$ characteristics in each design, which is also representative for $RS$: the jet was more straight in Design 1, while in Design 16 it was more curved and larger. This distribution remained qualitatively similar throughout the water column.

Table 3 illustrates maximum $TKE$ ($TKE_{max}$), average $TKE$ of the jet ($\overline{TKE_{jet}}$) and in the pool sides ($\overline{TKE_s}$); the percentage of pool area where $TKE \leq 0.05$ m$^2$/s$^2$ was also reported. The square root of pool average $\overline{TKE}$ was normalized using maximum pool velocity as a scale to obtain a dimensionless result.

In Design 1 $TKE_{max}$ reduced with increasing water depth $y_0$ (i.e the flow rate) of about 10-35% on $H_2$, and 2-5% on $H_4$, due to the decrease in maximum flow velocity. Maximum $TKE$ decreased by 15% as the free surface was approached, due to the slower jet velocity. In Design 16 a monotonic behavior was not easily identified, although maximum $TKE$ generally decreased as the free surface was approached and increased by increasing flow rate.

$\overline{TKE_{jet}}$ increased with the increase in flow rate (passing from $y_0 = 1$ to $y_0 = 1.5 - 2$ m) of about 4-15% (Design 1) and around 20% (Design 16), due to the more intensive turbulence. Average jet velocity was appreciably higher on $H_4$ with respect to $H_2$, with an increase of 9-25% for Design 1 and 10-13% for Design 16 from $H_2$ to $H_4$.

$\overline{TKE_s}$ reduced of 9-26% with flow rate in Design 1, while in Design 16 the decrease was only appreciable on $H_4$, and it corresponded to a decrease of 8-17% passing from $y_0 = 1$ m to $y_0 = 1.5 - 2$ m. $\overline{TKE_s}$ increased passing from $H_2$ to $H_4$ (thus it varied with $y$) in Design 1, while it decreased for Design 16 (1-17% of decrease). The increasing/decreasing trend with $y$ was due to the superimposition of two effects: the enlarging of the jet that tended to enhance $\overline{TKE_s}$, and the reduction of jet velocity that was perceived as a reduction in $\overline{TKE_s}$, since the jet had less energy to affect

the sides of the pool. These behaviors can be observed in Figs. 2, 3, 4. Hence, the final result depended on which effect was predominant. As a consequence, average $TKE$ in the resting zones of the pool was lower in Design 1 considering the lowest portion of the pool, but generally higher when considering the uppermost portion of the pool.

Normalized $TKE$ was appreciably lower for Design 1. This was confirmed by analyzing the area percentage with $TKE$ less than 0.05 $m^2/s^2$: it was higher in Design 1, except for $y_0 = 2$ m.

Comparing the two designs, it was possible to observe that the peaks of $TKE$ ($TKE_{max}$ was in the proximity of the slot) were lower in Design 16 (due to lower flow velocity) of 13-37%. $TKE_{jet}$ was higher in Design 16 on $H_2$ of 4-24%, but slower on $H_4$ of 5-10%. A similar behavior can be observed for $TKE_s$. In Design 16 $TKE_s$ was noticeably higher when considering $H_2$ (12-50% bigger), and only 3-9% lower on $H_4$ with respect to Design 1. The extension of resting zones (where $TKE \leq 0.05$ $m^2/s^2$) in Design 16 was lower by about 2-10% than in Design 1, except when $y_0 = 2$ m (8-10% wider). Anyway, low $TKE$ areas were in both cases wider than 30% of the pool area, consisting of 39% to 55% of the pool area for Design 1 and between 35% to 41% for Design 16.

### *3.5. Reynolds stresses in the pools*

Table 4 illustrates maximum $RS$ ($RS_{xy,max}$), and average jet ($\overline{RS_{xy,jet}}$) and pool sides ($\overline{RS_{xy,s}}$) $RS$. The area percentage with $RS$ in each cell $\leq 60$ $N/m^2$ is also reported.

Maximum $RS$ increased with flow rate; this was especially observed in Design 16, with an increase of more than 31% passing from $y_0 = 1$ m to

$y_0 = 1.5 - 2$ m. $RS$ decreased approaching the free surface, except for $y_0 = 2$ m; this again occurred especially for Design 16. The jet average $RS$ generally increased with flow rate by more than 30% with respect to the reference situation at $y_0 = 1$ m. $RS$ increased as the free surface was approached.

The average $RS$ in the resting zone was particularly affected by the flow rate when considering $H_2$. It increased when the free surface was approached, and this occurred especially for Design 1, with increases of more than 40%. The percentage area where $RS \leq 60$ N/m$^2$ was similar for all designs and conditions; it consisted of 89-97% of the pool area in Design 1 and between 91-97% of pool area in Design 16.

As for $TKE$, maximum $RS$ and jet average $RS$ occurred in Design 1. Indeed, in Design 1, maximum and average $RS$ were between 225-283 N/m$^2$ and 42-96 N/m$^2$, respectively, while in Design 16 $RS$ values were between 110-256 N/m$^2$ and 37-95 N/m$^2$, respectively. Average $RS_s$ were lower in Design 1, when considering the lowest portion of the pool, but higher when considering the uppermost one.

## 4. Discussion

Vertical slot fishways are considered the most efficient and least selective type of technical fishway solutions, and different designs exist. In this study the two most used designs were investigated (Design 1 and 16), with the aim of understanding with more details the flow field faced by fish. As reported in the Introduction, in VSF it is recommended that resting zones with $TKE \leq 0.05$ m$^2$/s$^2$ and $RS \leq 60$ N/m$^2$ be provided in 30% to 50%

of the pool, with velocities kept under 0.30 m/s. Eddies dimensions should be kept to adequate values compared to upstream migrants body lengths (Silva et al. 2012; Silva et al., 2015; Marriner at al., 2016).

The results achieved in this work were obtained by numerical simulations. The used numerical model was validated in Quaranta et al. (2016) based on results presented in Rajaratnam et al. (1992). In Quaranta et al. (2016), the CFD model was applied to Design 1 and 16 for a 10% bed slope setup, finding a good agreement between experiments and numerical results. The results presented here are also in good agreement with Khan (2006), Puertas et al. (2012) and Tarrade et al. (2008). In the following paragraphs, comparisons with existing literature and brief resumes of results will be discussed, with a focus on fish swimming performance.

The flow field was characterized by a main water jet between the slots, curved toward the left side of the pool. With regards to the jet, maximum velocity ($U_{max}$) and average jet velocity ($\overline{U_{jet}}$) decreased as flow rate increased (hence with $y_0$ increase). Hence an increase in flow rate is mostly seen as an increase in water level rather than in velocity, as confirmed by the equations relating the flow rate $Q$ with $y_0$ (Rajaratnam et al., 1992).

The jet inclination at the slot was 29° (Design 1) and 36° (Design 16), due to the different slot geometry. Therefore, in Design 16 the jet between the slots was more curved, as also shown in Puertas et al. (2012). In Design 1 the jet was not only straighter, but also faster: the faster jet improves the identification of the upstream path by fish, while it may increase fish energy expenditure somewhat. In both designs it could be observed the decrease of maximum jet velocity, with increase in jet width, as the free surface was

approached. This 3D effect has been also found by Khan (2006), and it can be considered the only 3D behavior of Design 1.

The curved configuration of the jet generated one eddy on the right and one eddy on the left side of the pool, each with a central core of lower velocities. The vortex core may potentially represent a trap for smaller migratory fish (Silva et al., 2012). Furthermore, due to the higher jet orientation, in Design 16 the eddy on the right approached a more circular shape and the jet affected the left side of the pool (which is larger than the right side) more than in Design 1, reducing the width of resting zones, that fish use for their rest.

In the flow field of Design 16, one further 3D characteristic was found, in addition to the enlargement of the jet approaching the free surface: the vortex splitting on the left side of the pool. From a certain water depth, two smaller eddies were generated from the splitting of the bigger one. Such smaller eddies are deemed to negatively affect fish behavior, since it generates two smaller eddies, more comparable with fish dimensions, and may disorientate them (Silva et al., 2012). Indeed, the transversal eddies dimension was 0.22-0.42 m, very detrimental especially for fish 0.15-0.40 m long.

In Tarrade et al. (2008) the vortex splitting has been shown also to occur in Design 1 at 10% slope, as also found in Quaranta et al. (2016), where the same numerical model here used was applied to Design 1 at 10% slope.

Areas $A$ with velocities lower than 0.3 m/s (as suggested by Marriner et al., 2016) were generally wider in Design 1, as it can be observed from

Table 1. This aspect is of high importance, especially when considering the need of resting by fish, after their use of burst speed. $A$ remained substantially constant in Design 1, while it was more variable in Design 16, due to the more variable flow field (vortex splitting). The explanation may be identified in the superimposition of two effects. The first effect is that the jet had lower velocity in Design 16, contributing to an increase in low velocity area percentage $A$ and a decrease in $\overline{U_s}$. Meanwhile, the jet was more curved (second effect), affecting the sides of the pool more than in Design 1. The latter effect contributed to the increase in flow velocity and turbulence at the sides of the pool, and thus to the decrease in areas $A$.

Maximum and average values of velocity and turbulent variables occurring in the jet were higher when considering Design 1. This means that fish can locally encounter more fatigue in swimming from one pool to the upstream one. However, because of the local validity of the maximum values, in order to draw more significant conclusions, the average jet values should be considered when dealing with the burst speed.

Considering average water velocities in resting zones, Design 1 is to be preferred, since resting areas are more quiet. Therefore, in the pool side fish have the possibility to rest more appropriately, with less fatigue and using lower prolonged speed. Hence fish can recover the energy they lost previously in the faster jet.

Referring to $RS$, the hydraulic configurations were very favorable for fish, since in more than 90% of the pool area $RS$ values were lower than the threshold value (60 N/m$^2$, Silva et al., 2011). Therefore, referring to $RS$, both hydraulic configurations were very favorable for fish.

Also $TKE$ values were lower than the threshold one (0.05 $m^2/s^2$, Silva et al., 2012) in more than 30% of the pool for both designs. The localization of maximum $TKE$ areas agrees well with Puertas et al. (2004) for Design 16. Although turbulent variables respected the threshold values, resting areas of Design 1 were less turbulent on $H_2$, and more turbulent on $H_4$. Thus, Design 1 has a very favorable behavior for fish swimming in the bottom portion of the pool. Furthermore, normalized $TKE$ was appreciably lower for Design 1, hence this design has a more dissipative effect, that makes it more preferable from a fish passage perspective.

In conclusion, the results obtained and presented in this work show that both designs are adequate for fish upstream migration, even if the larger eddy dimensions and the more uniform flow behavior make Design 1 more suitable for fish. As a consequence, Design 1 is recommended for engineering practice in relation to low-gradient VSF. It should be used in grayling-barbel regions, especially for potamodromous species with body length within the range 15-40 cm.

## 5. Conclusions

Two typical designs of vertical slot fishways were numerically simulated and investigated, using a bed slope of 5%. Three flow rates, as well as water depths, were investigated, and the flow field was compared along two planes. Results were compared with datasets found in literature, and the agreement was good.

Both designs satisfy prescriptions suggested by scientific literature and practitioners. Low $TKE$ and velocity areas were in both cases wider than

30% of the pool area, as recommended by Marriner et al. (2014). Referring to Reynolds stresses, hydraulic configurations were very favorable for fish, since in more than 90% of the pool area $RS$ values were lower than the threshold value (60 N/m$^2$).

However, results showed that the flow behavior inside the pools was different between the two designs. In Design 1 the flow field was qualitatively 2D, whereas in Design 16 it was more 3D, due to the eddy splitting and the less straightforward jet. The hydraulic characteristics in Design 16 changed more significantly with the vertical coordinate than in Design 1. Hence Design 1 should be preferred over Design 16 from an engineering point of view.

When considering the ecological point of view, conclusions can not be drawn easily. The flow field in the jet was more turbulent and velocities were faster in Design 1, but resting areas were more developed and quiet, providing more appropriate space with low velocities for fish to recover fish energy. Flow velocities in resting areas were appreciably higher in Design 16 of more than 16% with respect to Design 1. This means that fish need to use a higher burst speed and a lower prolonged speed in resting zones in Design 1, that were less turbulent and wider. Therefore, fish may encounter more fatigue in swimming from one pool to the upstream one in Design 1; meanwhile, they have the possibility to rest in the pool side, so that they can recover the energy that was lost in swimming in a more turbulent jet.

Considering turbulent kinetic energy, Design 1 is more dissipative. In Design 16 $TKE$ in resting zones was noticeably higher when considering $H_2$ (12-50% higher), and only 3-9% lower on $H_4$ with respect to Design 1.

The extension of resting zones (where $TKE \leq 0.05$ m$^2$/s$^2$) in Design 16 was lower by about 2-10% than in Design 1, except when $y_0 = 2$ m (8-10% wider).

As a consequence, it is reasonable to conclude that Design 1, even if 10-15% more expensive than Design 16 in terms of construction costs, generally should be considered the recommended design in relation to low-gradient VSF. This is due to its limited selectivity especially in grayling-barbel regions for potamodromous species with body length within the range 15-40 cm.

## 6. Bibliography


Barton, A., Keller, R., and Katopodis, C. 2008. A free surface model of a vertical slot fishway to numerically predict velocity and turbulence distributions. *American Fisheries Society Symposium*, **61**, 1-16.

Bunt, C. M., Castro-Santos, T., and Haro, A. 2012. Performance of fish passage structures at upstream barriers to migration. *River Research and Applications*, **28**, 457-478.

Calles, E.O. and Greenberg, L.A. 2009. Connectivity is a two-way street – the need for a holistic approach to fish passage problems in regulated rivers. *River Research and Applications*, **25**, 1268-1286.

Clay, C.H. 1995. Design of fishways and other fish facilities. *Second ed. Lewis Publishers, Boca Raton.*

Food and Agriculture Organization of the United Nations (FAO)

Deutscher Verband für Wasserwirtschaft und Kulturbau (DVWK). 2002. Fish passes – design, dimensions and monitoring. *Rome, FAO.*

Hatry, C., Binder, TR., Thiem, JD., Hasler, CT., Smokorowski, KE., Clarke, KD., Katopodis, C., and Cooke, SJ. 2016. The status of fishways in Canada: trends identified using the national canfishpass database. *Rev. Fish Biol. Fish.*, **23**, 271-281.

Heimerl, S., Hagmeyer, M., and Echteler, C. 2008. Numerical flow simulation of pool-type fishways: new ways with well-known tools. *Hydrobiologia*, **609**, 189-196.

Katopodis, C. 1992. Introduction to fishway design.

Katopodis, C. and Gervais, R. 2016. Fish swimming performance database and analyses. *Fisheries and Oceans Canada*, research document - 2016/002.

Katopodis, C. and Williams, J. 2012. The development of fish passage research in a historical context. *Ecological Engineering*, **48**, 8-18.

Khan, L. 2006. A three-dimensional computational fluid dynamics (CFD) model analysis of free surface hydrodynamics and fish passage energetics in a vertical-slot fishway. *North American Journal of Fisheries Management*, **26**, 255-267.

Laine, A., Kamula, R., and Hooli, J. 1998. Fish and lamprey passage in a combined denil and vertical-slot fishway. *Fisheries Management and Ecology*, **5**, 31-44.

Marriner, B.A., Baki, A.B.M., Zhu, D.Z., Cooke, S.J., and Katopodis, C. 2016. The hydraulics of a vertical slot fishway: A case study on the multi-species Vianney-Legendre fishway in Quebec, Canada. *Ecological Engineering*, **90**, 190-202.

Marriner, B.A., Baki, A.B.M., Zhu, D.Z., Thiem, J.D., Cooke, S.J., and Katopodis, C. 2014. Field and numerical assessment of turning pool hydraulics in a vertical slot fishway. *Ecological Engineering*, **63**, 88-101.

Olsson, E., Kreiss, G., and Zahedi, S. 2007. A conservative level set method for two phase flow II. *Journal of computational Physics*, **225(1)**, 785-807.

Plaut, I. 2012. Critical swimming speed: its ecological relevance. *Comparative Biochemistry and Physiology, part A*, **131**, 41-50.

Puertas, J., Cea, L., Bermúdez, M., Pena, L., Rodríguez, A., Rabunal, J.R., Balairón, L., Lara, A., and Aramburu, E. 2012. Computer application for the analysis and design of vertical slot fishways in accordance with the requirements of the target species. *Ecological Engineering*, **48**, 51-60.

Puertas, J., Pena, L., and Teijeiro, T. 2004. Experimental approach to the hydraulics of vertical-slot fishways. *Journal of Hydraulic Engineering*, **130**, 10-23.

Quaranta, E., Comoglio, C., Katopodis, C., and Revelli, R. 2016. Numerical simulations of flow field in vertical slot fishways. *Idra16, XXXV National Congress on Hydraulics and Hydraulic Structures, Bologna, Italy, 14-16 September, 749-752.*

Quaranta, E. and Revelli, R. 2016. Hydraulic behavior and performance of breastshot water wheels for different numbers of blades. *Hydraulic Engineering*, **143 (1)**, 04016072-1.

Rajaratnam, N., Katopodis, C., and Solanki, S. 1992. New designs for vertical-slot fishways. *Canadian Journal of Civil Engineering*, **19**, 402-414.

Santos, JM., Silva, AT., Katopodis, C., Pinheiro, PJ., Pinheiro, AN., Bochechas, J., and Ferreira, MT. 2016. Ecohydraulics of pool-type fishways: getting past the barriers. *Ecological Engineering*, **48**, 38-50.

Schmutz, S. and Mielach, C. 2013. Measures for ensuring fish migration at transversal structures. *International Commission for the Protection of the Danube River*.

Silva, A., Hatry, C., Thiem, J., Gutowsky, L., Hatin, D., Zhu, D., Dawson, J., Katopodis, C., and Cooke, S. 2015. Behaviour and locomotor activity of a migratory catostomid during fishway passage. *PLoS ONE*, **10(4)**: e0123051.

Silva, A., Santos, J., Ferreira, M., Pinheiro, A., and Katopodis, C. 2011. Effects of water velocity and turbulence on the behaviour of Iberian barbel (luciobarbus bocagei, Steindachner 1864) in an experimental pool-type fishway. *River Research and Applications*, **27**, 360-373.

Silva, A.T., Katopodis, C., Santos, J.M., Ferreira, M.T., and Pinheiro, A.N. 2012. Cyprinid swimming behaviour in response to turbulent flow. *Ecological Engineering*, **44**, 314-328.

Stuart, I. G. and Berghuis, A. P. 2002. Upstream passage of fish through a vertical-slot fishway in an Australian subtropical river. *Fisheries Management and Ecology*, **9**, 111-122.

Tarrade, L., Texier, A., David, L., and Larinier, M. 2008. Topologies and measurements of turbulent flow in vertical slot fishways. *Hydrobiologia*, **609 (1)**, 177-188.

Tritico, H.M and Cotel, A.J. 2010. The effects of turbulent eddies on the stability and critical swimming speed of creek chub (semotilus atromaculatus). *Journal of Experimental Biology*, 2284-2293.

White, L.J., Harris, J.H., and Keller, R.J. 2011. Movement of three non-salmonid fish species through a low-gradient vertical-slot fishway. *River Research and Applications*, **27 (4)**, 499-510.

Wu, S., Rajaratnam, N., and Katopodis, C. 1999. Structure of flow in vertical-slot fishway. *Journal of Hydraulic Engineering*, **125**, 352-360.

**List of Figures**

**Table 1.** Maximum flow velocity ($U_{max}$), average flow velocities in the jet ($\overline{U_{jet}}$) and in the area outside the jet ($\overline{U_s}$), and area percentage ($A$) with velocities lower than 0.3 m/s, on the plane $H_2 = 0.33y_0$ and $H_4 = 0.67y_0$. Units are reported.

| Plane | $y_0$ | $D1$ | | | | $D16$ | | | |
|---|---|---|---|---|---|---|---|---|---|
| | | $U_{max}$ | $\overline{U_{jet}}$ | $\overline{U_s}$ | $A$ | $U_{max}$ | $\overline{U_{jet}}$ | $\overline{U_s}$ | $A$ |
| | m | m/s | m/s | m/s | % | m/s | m/s | m/s | % |
| $H_2$ | 1.0 | 1.91 | 1.28 | 0.28 | 0.43 | 1.68 | 1.26 | 0.33 | 0.35 |
| | 1.5 | 1.75 | 1.22 | 0.31 | 0.46 | 1.62 | 1.21 | 0.36 | 0.43 |
| | 2.0 | 1.65 | 1.15 | 0.31 | 0.42 | 1.62 | 1.09 | 0.32 | 0.41 |
| $H_4$ | 1.0 | 1.80 | 1.16 | 0.28 | 0.48 | 1.56 | 1.07 | 0.38 | 0.47 |
| | 1.5 | 1.65 | 1.24 | 0.26 | 0.46 | 1.52 | 1.10 | 0.31 | 0.51 |
| | 2.0 | 1.67 | 1.20 | 0.28 | 0.47 | 1.60 | 1.07 | 0.27 | 0.52 |

**Table 2.** Maximum and minimum dimensions of each eddy core forming on the left and on the right of the water jet, on the plane $H_2 = 0.33y_0$ and $H_4 = 0.67y_0$. Units are reported.

| Plane | $y_0$ | $D1$ | | | | $D16$ | | | |
|---|---|---|---|---|---|---|---|---|---|
| | | left | | right | | left | | right | |
| | | $d_{max}$ | $d_{min}$ | $d_{max}$ | $d_{min}$ | $d_{max}$ | $d_{min}$ | $d_{max}$ | $d_{min}$ |
| | m | m | m | m | m | m | m | m | m |
| $H_2$ | 1.0 | 1.05 | 0.42 | 0.63 | 0.21 | 0.54 | 0.22 | 0.54 | 0.38 |
| | 1.5 | 0.98 | 0.54 | 0.71 | 0.27 | 0.52 | 0.29 | 0.69 | 0.23 |
| | 2.0 | 0.79 | 0.42 | 0.63 | 0.21 | 0.90 | 0.42 | 0.59 | 0.30 |
| $H_4$ | 1.0 | 0.79 | 0.37 | 0.53 | 0.26 | 0.67 | 0.22 | 0.33 | 0.22 |
| | 1.5 | 0.74 | 0.27 | 0.54 | 0.22 | 0.68 | 0.23 | 0.51 | 0.28 |
| | 2.0 | 0.84 | 0.32 | 0.42 | 0.16 | 0.86 | 0.34 | 0.57 | 0.34 |

**Table 3.** Maximum $TKE$ ($TKE_{max}$), jet average $TKE$ ($\overline{TKE_{jet}}$), pool's sides average $TKE$ ($\overline{TKE_s}$), dimensionless value of $TKE$, and area percentage $A$ where $TKE$ is lower than 0.05 $m^2/s^2$, on the plane $H_2 = 0.33y_0$ and $H_4 = 0.67y_0$. Units are reported.

| Plane | $y_0$ | $D1$ | | | | | $D16$ | | | | |
|---|---|---|---|---|---|---|---|---|---|---|---|
| | m | $TKE_{max}$ $m^2/s^2$ | $\overline{TKE_{jet}}$ $m^2/s^2$ | $\overline{TKE_s}$ $m^2/s^2$ | $\frac{\sqrt{\overline{TKE}}}{v_{max}}$ - | $A$ % | $TKE_m$ $m^2/s^2$ | $\overline{TKE_{jet}}$ $m^2/s^2$ | $\overline{TKE_s}$ $m^2/s^2$ | $\frac{\sqrt{\overline{TKE}}}{v_{max}}$ - | $A$ % |
| $H_2$ | 1.0 | 0.40 | 0.162 | 0.065 | 0.159 | 0.39 | 0.32 | 0.169 | 0.073 | 0.191 | 0.35 |
| | 1.5 | 0.36 | 0.147 | 0.048 | 0.147 | 0.55 | 0.31 | 0.154 | 0.072 | 0.177 | 0.40 |
| | 2.0 | 0.26 | 0.170 | 0.059 | 0.160 | 0.39 | 0.34 | 0.211 | 0.077 | 0.177 | 0.42 |
| $H_4$ | 1.0 | 0.35 | 0.177 | 0.077 | 0.156 | 0.43 | 0.22 | 0.158 | 0.072 | 0.188 | 0.39 |
| | 1.5 | 0.34 | 0.198 | 0.066 | 0.166 | 0.45 | 0.26 | 0.186 | 0.060 | 0.187 | 0.41 |
| | 2.0 | 0.33 | 0.204 | 0.064 | 0.164 | 0.41 | 0.33 | 0.192 | 0.066 | 0.172 | 0.45 |

**Table 4.** Maximum Reynolds stresses $RS_{xy,max}$, average Reynolds stresses in the jet $\overline{RS_{xy,jet}}$ and in the pool's sides $\overline{RS_{xy,s}}$, and area percentage with $RS \leq 60$ $N/m^2$, on the plane $H_2 = 0.33y_0$ and $H_4 = 0.67y_0$. Units are reported.

| Plane | $y_0$ | $D1$ | | | | $D16$ | | | |
|---|---|---|---|---|---|---|---|---|---|
| | m | $RS_{xy,max}$ $N/m^2$ | $\overline{RS_{xy,jet}}$ $N/m^2$ | $\overline{RS_{xy,s}}$ $N/m^2$ | $A$ % | $RS_{xy,max}$ $N/m^2$ | $\overline{RS_{xy,jet}}$ $N/m^2$ | $\overline{RS_{xy,s}}$ $N/m^2$ | $A$ % |
| $H_2$ | 1.0 | 261.4 | 49.7 | 11.2 | 0.91 | 195.4 | 40.9 | 11.8 | 0.96 |
| | 1.5 | 282.6 | 41.9 | 10.0 | 0.96 | 192.8 | 36.6 | 14.6 | 0.96 |
| | 2.0 | 259.0 | 84.6 | 13.7 | 0.89 | 256.4 | 95.3 | 16.9 | 0.97 |
| $H_4$ | 1.0 | 224.7 | 60.0 | 16.7 | 0.97 | 110.8 | 49.9 | 12.5 | 0.94 |
| | 1.5 | 242.5 | 81.1 | 17.7 | 0.96 | 161.3 | 74.7 | 12.0 | 0.95 |
| | 2.0 | 272.9 | 96.4 | 16.6 | 0.96 | 246.7 | 87.7 | 14.2 | 0.91 |

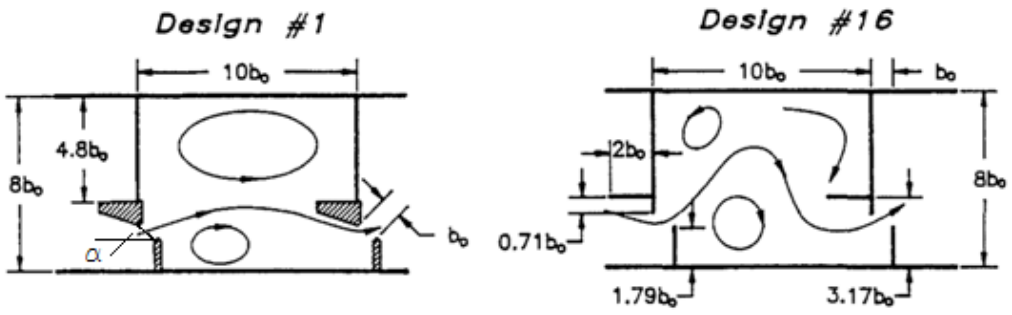


**Fig. 1.** Geometric features of Design 1 and Design 16 of VSF (adapted from Rajaratnam et al., 1992). Design 16 differs from Design 1 in the geometry of the baffles, whereas for both designs the pool dimensions are the same. In the CFD model the reference value $b_0 = 0.30$ m was used.

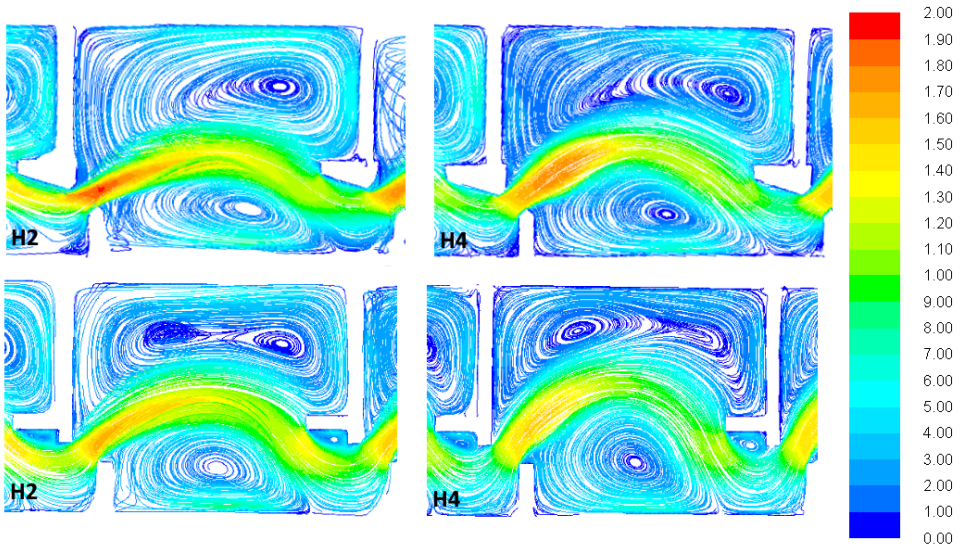


**Fig. 2.** Velocity flow field of Design 1 (top) and 16 (bottom) for $y_0 = 1$ m on planes $H_2$ and $H_4$. Units in m/s.

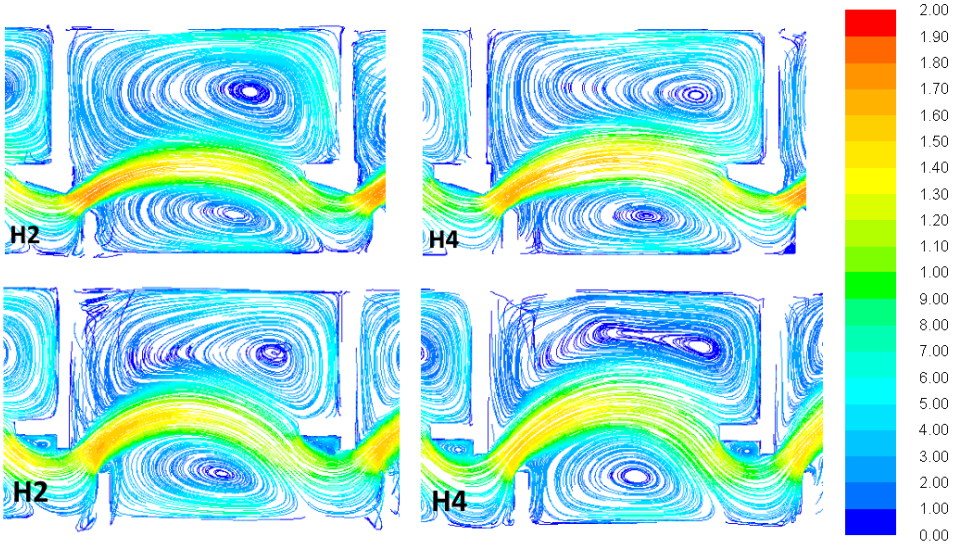


**Fig. 3.** Velocity flow field of Design 1 (top) and 16 (bottom) for $y_0 = 1.5$ m on planes $H_2$ and $H_4$. Units in m/s.

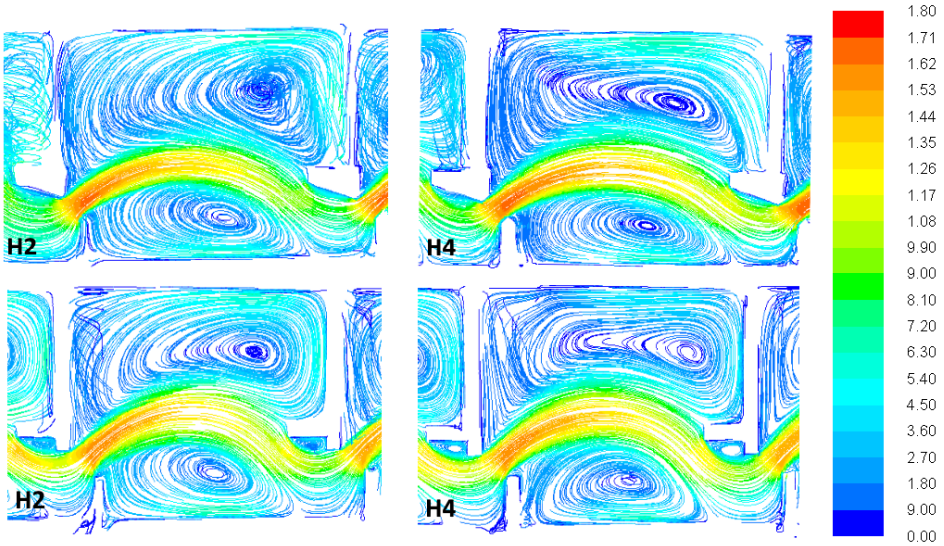


**Fig. 4.** Velocity flow field of Design 1 (top) and 16 (bottom) for $y_0 = 2$ m on planes $H_2$ and $H_4$. Units in m/s.

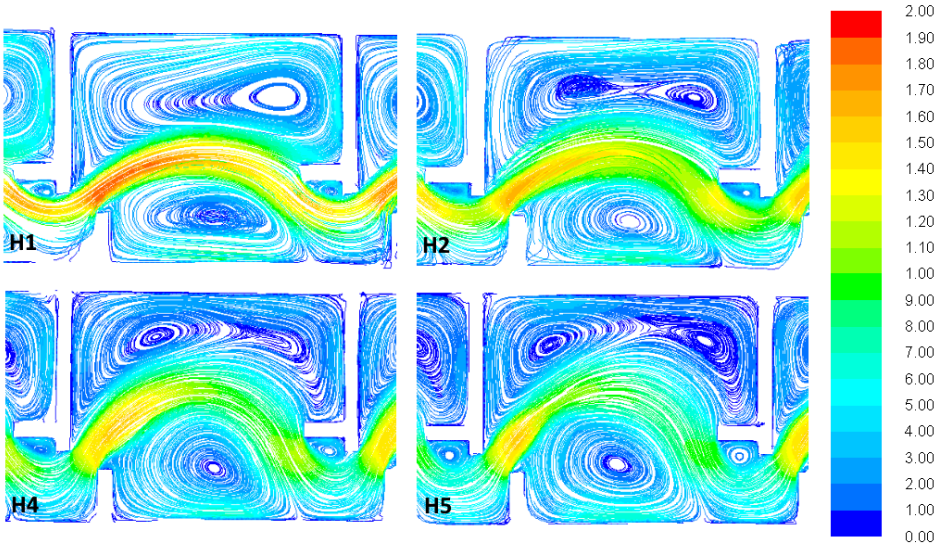


**Fig. 5.** Velocity flow field of Design 16 for $y_0 = 1$ m on different planes. Units in m/s.

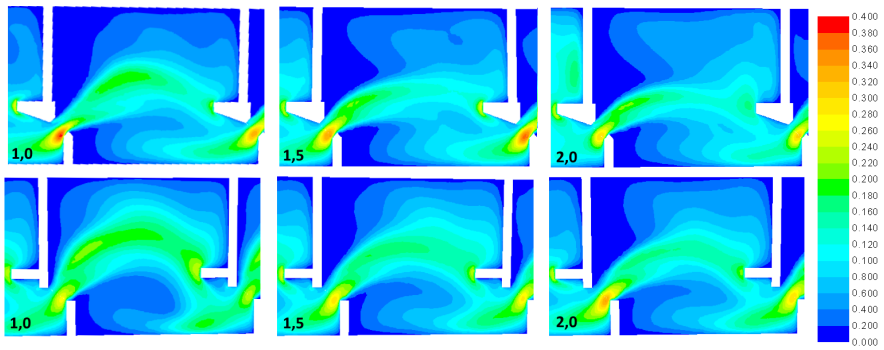


**Fig. 6.** Turbulent kinetic energy for Design 1 (top) and Design 16 (bottom) at $y_0 = 1.0, 1.5, 2.0$ m along the representative plane $H_3$ at $y = 0.5y_0$. The $TKE$ field remains qualitatively similar along the water column. Units in $\mathrm{m}^2/\mathrm{s}^2$.